

First-principles, atomistic thermodynamics for oxidation catalysis

Karsten Reuter and Matthias Scheffler

Fritz-Haber-Institut der Max-Planck-Gesellschaft, Faradayweg 4-6, D-14195 Berlin, Germany and

(Received 16 October)

Present knowledge of the function of materials is largely based on studies (experimental and theoretical) that are performed at low temperatures and ultra-low pressures. However, the majority of everyday applications, like e.g. catalysis, operate at atmospheric pressures and temperatures at or higher than 300 K. Here we employ *ab initio*, atomistic thermodynamics to construct a phase diagram of surface structures in the (T, p) -space from ultra-high vacuum to technically-relevant pressures and temperatures. We emphasize the value of such phase diagrams as well as the importance of the reaction *kinetics* that may be crucial e.g. close to phase boundaries.

PACS numbers: PACS: 82.65.Mq, 68.35.Md, 68.43.Bc

The main prerequisites for reaching a microscopic understanding of heterogeneous catalysis are the identification of the composition and geometry of the catalyst surface and the determination of the various chemical reactions that take place under realistic conditions. Unfortunately, most *Surface Science* experimental techniques are difficult if not impossible to use at the pressures (of the order of one atmosphere) and temperatures (often higher than 300 K) that are typically applied in steady-state catalysis. Therefore, what is considered to be important elementary processes at the catalyst surface (e.g. dissociation, diffusion, and chemical reactions) has usually been concluded from chemical intuition and extensive knowledge from ultra-high vacuum (UHV) experiments. However, several studies revealed the danger of this approach (see e.g. Ref. [1] and references therein), and the need to reliably bridge the temperature and pressure gap between UHV and “real life” is probably the main challenge in modern *Surface Science*.

In *ab initio* theory the consideration of high temperature and high pressure can be achieved by explicitly taking into account the surrounding gas phase in terms of “*ab initio*, atomistic thermodynamics” (cf. e.g. Refs. [2, 3, 4, 5, 6]). This is also an appropriate (first) approach to steady-state catalysis, which is often run close to thermodynamic equilibrium (or a constrained equilibrium) to prevent catalyst degradation. We will qualify this statement below when analyzing our results. In the following we show how the combination of thermodynamics and density-functional theory (DFT) can be applied to obtain the lowest-energy surface structures in a (constrained) equilibrium with the surrounding gas phase, thus enabling us to construct a (T, p) -diagram of the stability regions (or metastability regions) of different surface phases. We use the example of CO oxidation over a $\text{RuO}_2(110)$ model catalyst to illustrate the concepts and conclusions that can be derived from such an *ab initio* surface phase diagram.

At given temperature, T , and partial pressures, $\{p_i\}$, the stable surface structure is the one that has the

lowest surface energy, $\gamma(T, \{p_i\}) = 1/A[G(T, \{p_i\}) - \sum_i N_i \mu_i(T, p_i)]$. Here, $G(T, \{p_i\})$ is the Gibbs free energy of the finite crystal, N_i and $\mu_i(T, p_i)$ are number and chemical potential of the species of the i th type, and $\gamma(T, \{p_i\})$ is measured in energy per unit area by dividing through the surface area, A . The surface free energy is thus a function of the chemical potentials of all species in the system, e.g. in the present application to CO oxidation over $\text{RuO}_2(110)$ we have three $\mu_i(T, p_i)$ corresponding to the three chemical elements: Ru, C, and O. Considering that the surface is not only in equilibrium with the gas phase, but also in equilibrium with the underlying metal oxide, implies that the chemical potentials of Ru and O are not independent variables but tied by the Gibbs free energy of the bulk oxide. As a consequence, the surface free energy depends only on two chemical potentials, which we choose to be those of O and CO. Because chemical potentials are directly related to temperature and partial pressure, a comparison to the whole range of experimentally accessible gas phase conditions is achieved.[6, 7] Here, we note that the above description refers to a *constrained* thermodynamic equilibrium only with the reactants, because it assumes that the O_2 and CO gas phase are independent *reservoirs*, and the direct (non catalytic) formation of CO_2 in the gas phase can be ignored because of its negligible rate.

As shown previously [6], for RuO_2 it is a good approximation to assume that the vibrational contributions to the Gibbs free energy, $G(T, \{p_i\})$, nearly equal the corresponding terms of the bulk oxide. We will therefore replace these quantities by the corresponding total energies, which are calculated using DFT. We use the generalized gradient approximation (GGA) for the exchange-correlation functional [9], and the all-electron Kohn-Sham equations are solved by employing the full-potential linear augmented plane wave (FP-LAPW) method [10, 11]. The high accuracy of these calculations (cf. Ref. [6]) implies that the numerical accuracy of the relative $\gamma(T, \{p_i\})$ is better than $\pm 5 \text{ meV}/\text{\AA}^2$. We also note that using the local-density approxima-

tion (LDA) as exchange-correlation functional gives essentially the same result for the surface phase diagram (cf. Fig. 2). Thus, the DFT accuracy for this system's surface phase diagram is very high, partly due to the fact that it follows only from energy *differences*.

Ruthenium is well known to exhibit an exceptionally high activity for the catalytic oxidation of CO, with turnover rates exceeding those of the more commonly employed materials like Rh, Pd, or Pt.[12, 13] For Ru(0001) this high activity could be related to RuO₂(110) oxide patches that are formed in the reactive environment.[14, 15, 16] The atomic arrangement at RuO₂(110) can be described by starting from the stoichiometric surface (see the orange-framed inset in Fig. 1, labeled O^{br}/–). There are two different oxygen atoms at this surface: threefold-bonded O^{3f} (as is an O atom in bulk RuO₂) and twofold bridge-bonded O^{br}. Likewise, there are two different surface Ru atoms, one of which is bonded to six oxygen neighbors (as is a Ru atom in bulk RuO₂), and one is bonded to only five O neighbors. The latter represents a “coordinatively unsaturated site” and is called Ru^{cus}. The bulk stacking sequence would be continued by adsorbing additional oxygen atoms on top of the Ru^{cus} atoms. This gives the red-framed oxygen-rich geometry, O^{br}/O^{cus}. The adsorption energy for a single O atom on the Ru^{cus} atom of the O^{br}/– surface is calculated to be exothermic by 1.2 eV/adatom (at $\mu_O = 0$ eV)[17]. And the energy of an oxygen vacancy in the O^{br}/– surface is calculated to be endothermic by 2.5 eV/vacancy (removing a O^{br} atom) and ≈ 3.5 eV/vacancy (removing a O^{3f} atom) at $\mu_O = 0$ eV[17]. Removing all bridge-bonded oxygen atoms from the O^{br}/– surface gives the black-framed, oxygen-poor geometry –/– in Fig. 1, which represents the third possible (1×1) termination of RuO₂(110).

The μ_O scale can be converted into a pressure scale at any chosen temperature,[6, 7] and this is noted at the top of Fig. 1 for $T = 600$ K, a typical annealing temperature used experimentally in this system [15, 16]. From the computed surface free energies of the aforementioned three RuO₂(110) terminations, we obtain that even at the lowest possible O₂ pressures, O atoms will at least occupy the bridge sites, leading to the stoichiometric surface termination (the orange line tagged as O^{br}/– in Fig. 1). At even lower $\mu_O(T, p_{O_2})$ than the O-poor boundary in Fig. 1, RuO₂ will decompose into Ru metal.[6]

We now consider the presence of CO as a second species, discussing the surface structure of RuO₂ in the constrained equilibrium with a CO and O₂ gas phase. For this we computed what we believe are all possible (1×1) surface phases including O and CO at the surface.[18] Figure 1 shows the corresponding surface energies in the CO-rich limit for μ_{CO} of three CO containing structures that will play a role in the later discussion. In this CO-rich limit and if the O chemical potential is below -1.2 eV, CO is transformed into graphite and $1/2$ O₂.

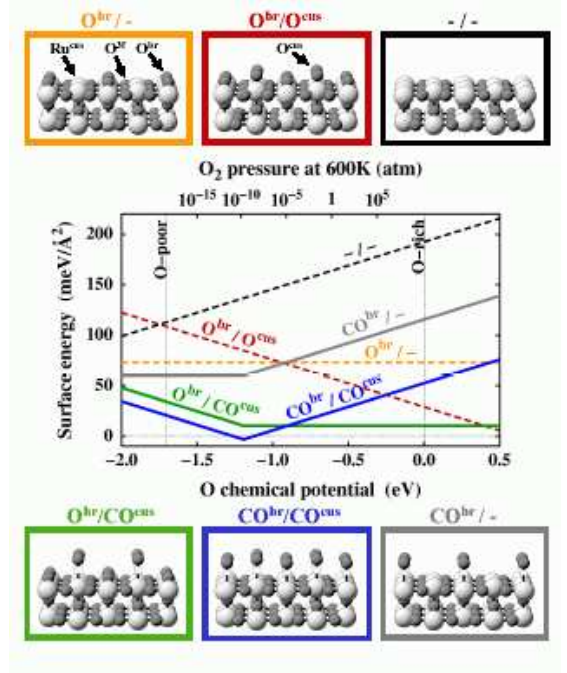


FIG. 1: Surface free energies, $\gamma(T, \{p_i\})$, in the experimentally accessible range of the oxygen chemical potential.[6, 7] Shown are three RuO₂(110) terminations (dashed lines and black, red, and orange insets), and the three most stable CO containing surface phases for the CO-rich limit (solid lines and gray, green, and blue insets). The labels note whether bridge or cus sites are occupied by O or CO, or are empty (–). Ru atoms are drawn as light, large, O atoms as dark, small, and C atoms as white, small spheres.

This is why the CO related (gray, blue, and green) lines in Fig. 1 exhibit a kink at $\mu_O = -1.2$ eV. As apparent from Fig. 1 a phase with CO occupying all bridge sites (the gray line tagged as CO^{br}/–) is barely more stable than the hitherto discussed pure O-terminations; and occupation of also the cus sites (CO^{br}/CO^{cus}) leads to a (meta)stable phase only at low O chemical potential. Towards higher μ_O we find a third relevant geometry, that exhibits O atoms at the bridge sites and CO at the cus sites, (O^{br}/CO^{cus}).

If we now in addition to μ_O investigate the dependence on μ_{CO} , Fig. 1 turns into a complicated three-dimensional plot. We therefore present our results by showing only the lowest-energy surface structures (concluded from many calculations of the type shown in Fig. 1 for any value of μ_{CO}). Figure 2 displays this central result of our study from which the stability regions of all surface phases in (constrained) equilibrium with an environment formed by O₂ and CO can be seen. At very low CO chemical potential corresponding to very low CO pressure in the gas phase, we recover our results obtained for RuO₂(110) just in equilibrium with an O₂ environment (dashed lines in Fig. 1): At low O chemical potential we find the stoichiometric termination with O

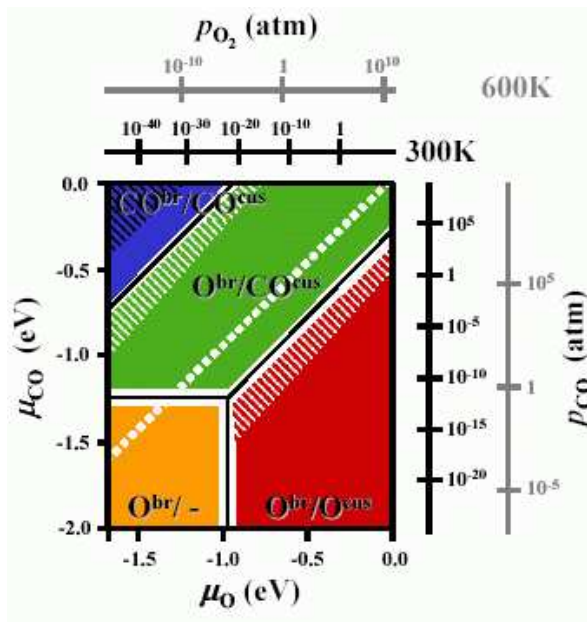


FIG. 2: Regions of the lowest-energy structures in (μ_O, μ_{CO}) -space (see Fig. 1 for the nomenclature). The additional axes give the corresponding pressure scales at $T = 300$ K and 600 K. In the blue-hatched region gas phase CO is transformed into graphite. Regions that are particularly strongly affected by kinetics are marked by white hatching (see text).

at bridge sites, while towards higher O_2 pressures the O-rich termination with O additionally located at the cus sites becomes more stable. Increasing the CO content in the gas phase, CO is first bound at the cus sites. This is easier at low O chemical potentials, where these sites are free. At higher μ_O oxygen atoms also compete for cus sites, which is why the O^{br}/CO^{cus} phase becomes only more stable than the O^{br}/O^{cus} phase at progressively higher CO chemical potentials, cf. Fig. 2. Finally, at a high CO and low O chemical potential in the upper-left corner of Fig. 2, we find that CO is also stabilized at the bridge sites (instead of O), leading to a completely CO covered surface (CO^{br}/CO^{cus}).

The knowledge of such a phase diagram (Fig. 2) is a first, important step towards an understanding where in $(T, \{p_i\})$ -space catalysis may be most efficient, but in parallel it also allows to systematically discuss under which gas phase conditions our constrained thermodynamic equilibrium approach may break down: We recall that the imposed constraints are that (i) in the gas phase the two molecules will not react to CO_2 , which is appropriate because the free-energy barrier is significant. Thus, CO_2 is only formed at the catalyst surface from where it will desorb immediately. Furthermore, it is assumed that (ii) the CO_2 formation at the surface is slower than other adsorption and desorption processes, so that the surface can maintain its equilibrium with the reactant gas phase. Finally, (iii) the gas phase should

not affect the stability of the RuO_2 bulk structure.

With respect to the latter point, we note that for $\mu_{CO} > \mu_O + \Delta$, RuO_2 will decompose into Ru metal ($\Delta^{th} = 0.06$ eV, see the dotted white line in Fig. 2; and $\Delta^{exp} = 0.26$ eV[8]). Thus, a noticeable part of Fig. 2 (the blue and most of the upper-left green region) refers to metastable situations and will not prevail for long under realistic conditions. As for the remaining part of the phase diagram, it is clear from the pressure scales in Fig. 2 that the stoichiometric surface (orange region, denoted as $O^{br}/-$), that had been observed in UHV experiments, is not very important under high-pressure, catalytically relevant conditions. Obviously, for oxidation catalysis it is important that both reactants (here CO and O) are adsorbed at the surface. In this respect, the green region (O^{br}/CO^{cus}) appears to be the most relevant one at first glance, and we have to ask if our remaining assumption (ii) of the constrained thermodynamic approach is appropriate here: If the reaction $CO^{cus} + O^{br} \rightarrow CO_2$ were faster than the dissociative adsorption of O_2 , adsorbed CO would rapidly eat away bridge-bonded oxygen atoms, and surface kinetic effects would render the oxygen concentration much lower than the full monolayer that is behind the atomic structure of the green region. Fortunately, for this region the CO_2 formation energy barrier is calculated to be noticeable (1.2 eV, in agreement with Ref. [19]), and the energy to create vacancies in the O-bridge layer is high (see above). Correspondingly, the thermodynamic approach seems to be valid here.

The question remains where in (T, p) -space do we expect the RuO_2 catalysis to be most efficient? In this context we note that a so-called stable phase is not stable on an atomistic scale, but represents an average over many processes such as dissociation, adsorption, diffusion, association and desorption. As all these processes and their interplay [1] are of crucial importance for catalysis, regions in (T, p) -space where such fluctuations are particularly pronounced can be expected to be most important. This is the case close to the boundaries between different phases: At finite temperatures, the transition into a neighboring phase occurs not abruptly in (μ_O, μ_{CO}) -space, but over a pressure range in which the other phase gradually becomes more populated. The resulting phase coexistence at the catalyst surface may then lead to a significantly enhanced dynamics, in which even additional reaction mechanisms can take place and/or (dynamic) domain pattern formation may occur. Assuming a canonic distribution we estimated in Fig. 2 the region on both sides of the boundaries in which the respective other phase is present at least at a 10% concentration at room temperature (white areas). From the given pressure scales we see that of particular interest for catalysis is the green/red boundary between the O^{br}/CO^{cus} and O^{br}/O^{cus} phases, where oxygen atoms and CO molecules compete for the same site, i.e. the cus site.

In fact, in this phase-transition region and in the neigh-

boring hatched part of the red phase in Fig. 2, assumption (ii) of our constrained equilibrium theory is not valid and the oxygen coverage will presumably be noticeably lower than what the present approach suggests: Under these conditions adsorbed CO will react with O^{cus} , and the filling of empty sites with CO will be fast, whereas the filling with oxygen atoms will be slow. In this region high catalytic activity is expected and we note that here the coverage and structure (i.e., the very dynamic behavior) must be modeled by statistical mechanics. However, this is not the point of the present paper that aims to *identify* the catalytically active region in $(T, \{p_i\})$ -space, and the neighboring stable phases. The exceptionally high turnover rates over working Ru catalysts were measured for conditions, where both gas phase species are present at ambient pressures and about equal partial pressures [12, 13, 20], i.e. for conditions which lie very close to the red-green boundary in Fig. 2, in accordance with our conclusions.

Finally, Fig. 2 also shows that the pressure gap can be bridged when sufficient information about the stability regions of the various surface phases is available, i.e. when it is assured that one stays within one phase region or along one particular phase boundary. A decrease of ambient gas phase pressures over several orders of magnitude maintaining an about equal partial pressure ratio of O_2 and CO will e.g. still result in conditions rather close to the green-red boundary in Fig. 2, and similar reaction rates have indeed recently been noticed by Wang *et al.* [21] when comparing corresponding UHV steady-state kinetic data with high pressure experiments of Zang and Kisch [22]. Yet, from Fig. 2 it is also clear, that without knowledge of a $(T, \{p_i\})$ -phase diagram a naive bridging of the pressure gap by simply maintaining an arbitrary constant partial pressure ratio of the reactants can easily lead to crossings to other phase regions and in turn to incomparable results.

In conclusion we computed the phase diagram of surface structures of $RuO_2(110)$ in constrained equilibrium with a gas phase of O_2 and CO. Depending on the temperature and partial pressures of these reactants, several stable and/or metastable surface phases are found. The presented calculations are of highest quality (at this time), but the employed GGA is an approximation, and the resulting uncertainty may well be of the order ± 100 K. Fortunately this should affect our conclusions only little. In particular, our study shows that if one stays within the region of one phase or along one particular phase boundary, a reliable bridging of the pressure gap is possible. While we emphasize the importance of such phase diagrams (Fig. 2), we also note that understanding of the full catalytic cycle requires a kinetic modeling, but for a system as complex as the present one, this is not yet possible.

Regions in $(T, \{p_i\})$ -space that exhibit enhanced ther-

mal fluctuations, i.e. where the dynamics of atomistic processes is particularly strong, are particularly interesting for the function of surfaces under realistic conditions - not only for the example discussed in this paper. The described approach identifies such regions close to boundaries in the computed surface phase diagram, where we correspondingly expect a particularly high catalytic activity. For our example of the CO oxidation reaction over $RuO_2(110)$ this conclusion is indeed consistent with existing data [12, 13, 20].

-
- [1] C. Stampfl *et al.*, Surf. Sci. **500**, 368 (2002).
 - [2] C.M. Weinert and M. Scheffler, In: *Defects in Semiconductors*, H.J. von Bardeleben (Ed.). Mat. Sci. Forum **10-12**, 25 (1986).
 - [3] M. Scheffler, In: *Physics of Solid Surfaces - 1987*, J. Koukal (Ed.). Elsevier, Amsterdam (1988).
 - [4] E. Kaxiras *et al.*, Phys. Rev. B **35**, 9625 (1987).
 - [5] G.-X. Qian, R.M. Martin and D.J. Chadi, Phys. Rev. B **38**, 7649 (1988).
 - [6] K. Reuter and M. Scheffler, Phys. Rev. B **65**, 035406 (2002).
 - [7] We use $\mu_O(T, p_{O_2}) = \frac{1}{2}\mu_{O_2}(T, p^0) + \frac{1}{2}k_B T \ln(p_{O_2}/p^0)$ and $\mu_{CO}(T, p_{CO}) = \mu_{CO}(T, p^0) + k_B T \ln(p_{CO}/p^0)$ to relate the chemical potential to temperature and partial pressure. The chemical potentials of O_2 and CO at standard pressure, $p^0 = 1$ atm, are tabulated e.g. in Ref. [8].
 - [8] JANAF Thermochemical Tables, D.R. Stull and H. Prophet, 2nd ed., U.S. Nat. Bureau of Standards, Washington, D.C. (1971).
 - [9] J.P. Perdew, K. Burke and M. Ernzerhof, Phys. Rev. Lett. **77**, 3865 (1996).
 - [10] P. Blaha, K. Schwarz and J. Luitz, WIEN97, Techn. Univ. Wien, Austria (1999). ISBN 3-9501031-0-4
 - [11] The FP-LAPW numerical parameters are: $R_{Ru}^{MT} = 1.8$ bohr, $R_O^{MT} = 1.1$ bohr, $R_C^{MT} = 1.0$ bohr, $E_{wf}^{max} = 20$ Ry, $E_{pot}^{max} = 169$ Ry. The \mathbf{k} integrations are replaced by a sum over 50 \mathbf{k} -points in the (1×1) Brillouin-zone.
 - [12] N.W. Cant, P.C. Hicks and B.S. Lennon, J. Catal. **54**, 372 (1978).
 - [13] C.H.F. Peden and D.W. Goodman, J. Phys. Chem. **90**, 1360 (1986).
 - [14] A. Böttcher *et al.*, J. Phys. Chem. B **101**, 11185 (1997).
 - [15] H. Over *et al.*, Science **287**, 1474 (2000).
 - [16] Y.D. Kim *et al.*, Top. Catal. **14**, 95 (2001).
 - [17] The zero of μ_O is set at $1/2 E_{O_2}$, where E_{O_2} is the total energy of a single O_2 molecule. This value of μ_O thus refers to the most oxygen-rich situation.
 - [18] In addition to the adsorption sites depicted in Fig. 1 we also tested other configurations, including more dilute phases, computed in bigger supercells. Details of all these studies will be described elsewhere.
 - [19] Z.P. Liu, P. Hu and A. Alavi, J. Chem. Phys. **114**, 5956 (2001).
 - [20] C.Y. Fan *et al.*, J. Chem. Phys. **114**, 10058 (2001).
 - [21] J. Wang *et al.*, J. Phys. Chem. B **106**, 3422 (2002).
 - [22] L. Zang and H. Kisch, Angew. Chemie **112**, 4075 (2000).